NASA Technical Memorandum 4633

25 p

Pressure-Sensing Performance of Upright Cylinders in a Mach 10 Boundary-Layer

Steven Johnson and Kelly Murphy

July 1994

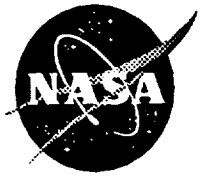

NASA Technical Memorandum 4633

Pressure-Sensing Performance of Upright Cylinders in a Mach 10 Boundary-Layer

Steven Johnson
Dryden Flight Research Center
Edwards, California

and

Kelly Murphy
NASA Langley Research Center
Hampton, Virginia

National Aeronautics and
Space Administration

Office of Management

Scientific and Technical
Information Program

1994

CONTENTS

ABSTRACT

An experimental research program to provide basic knowledge of the pressure-sensing performance of upright, flush-ported cylinders in a hypersonic boundary layer is described. Three upright cylinders of 0.25-, 0.5-, and 1-in. diameters and a conventional rake were placed in the test section sidewall boundary layer of the 31 Inch Mach 10 Wind Tunnel at NASA Langley Research Center, Hampton, Virginia. Boundary-layer pressures from these cylinders were compared to those measured with a conventional rake. A boundary-layer thickness-to-cylinder-diameter ratio of 8 proved sufficient to accurately measure an overall pressure profile and ascertain the boundary-layer thickness. Effects of Reynolds number, flow angularity, and shock wave impingement on pressure measurement were also investigated. Although Reynolds number effects were negligible at the conditions studied, flow angularity above 10° significantly affects the measured pressures. Shock wave impingement was used to investigate orifice-to-orifice pressure crosstalk. No crosstalk was measured. The lower pressure measured above the oblique shock wave impingement showed no influence of the higher pressure generated at the lower port locations.

INTRODUCTION

Measuring boundary-layer stagnation pressures in a high-stagnation temperature environment constitutes a fundamental measurement problem for future hypersonic flight vehicles. In the past for flight speeds up to Mach 6, conventional rakes were successfully used to acquire boundary-layer pitot pressure surveys.[1,2,3,4] For the hypersonic flight regime above Mach 6, however, the practice of using conventional rake designs which employ protruding pitot tubes is complicated because of the likelihood of heat-related failure of the pitot tubes.

A rake without the protruding pitot tubes is an attractive alternative to the conventional rake design. Survivability would be enhanced by eliminating the protruding pitot tubes, but the resulting pressure-sensing accuracy is unknown. Such a rake may introduce measurement inaccuracies associated with probe geometry, wall influence, Reynolds number, flow angularity, and shock wave effects that would not be evident with a conventional rake. In addition, orifice crosstalk, a situation where a low pressure measured at one location on a boundary-layer probe may be influenced by a high pressure measured at another location, may occur.

An early study of a rake without protruding pitot tubes showed promise. A NASA Ames Research Center, Moffett Field, California, study in a Mach 3 wind tunnel turbulent boundary layer comparing boundary-layer pitot profiles measured by a single traversing probe and a probeless rake found only a 2 percent difference.[5] This test was limited in that it was performed at a relatively low Mach number, with no flow angularity, and did not investigate probe geometry effects.

The NASA Dryden Flight Research Center, Edwards, California, and NASA Langley Research Center (NASA Langley), Hampton, Virginia, conducted the first such experimental investigation of the pressure-sensing performance of upright cylinders in a Mach 10 boundary layer. In this study, upright cylinders of varying diameters and a conventional rake were placed in the test section sidewall boundary layer of the NASA Langley 31 Inch Mach 10 Wind Tunnel. The boundary-layer pressures measured using three upright cylinders of 0.25-, 0.5-, and 1-in. diameter were compared to the boundary-layer pressures measured with a conventional rake. Effects of flow angularity and Reynolds number on pressure measurement were also investigated. To study potential crosstalk effects, a shock wave was impinged on the 1-in. diameter cylinder, and the pressures above and below the shock impingement location were compared. This technical memorandum describes the test articles, boundary-layer pressure measurement comparisons, flow angularity results, and oblique shock wave impingement pressure profile comparisons.

NOMENCLATURE

ESP	electronically scanned pressure
ID	inner diameter
M	Mach number
NASA Langley	National Aeronautics and Space Administration, Langley Research Center, Hampton, Virginia
OD	outer diameter
Re	unit Reynolds number
T	Temperature, °R
γ	ratio of specific heats
x	boundary-layer thickness-to-cylinder-diameter ratio
y	deviation thickness expressed as a percent of boundary-layer thickness

Subscripts

o	reservoir conditions
∞	free-stream conditions

EXPERIMENTAL METHODS

The NASA Langley 31 Inch Mach 10 Wind Tunnel was used for this work. This blow-down wind tunnel has a fixed geometry, three-dimensional contoured nozzle with a 31 in. square test section. The test gas, dry air, was heated to a nominal temperature of 1800 °R to prevent air liquefaction in the test section. The maximum reservoir pressure was approximately 1500 psia. The test section unit Reynolds number varied between 0.5 and 2 million/ft, depending on the value of the reservoir pressure.

A test article was supported on a hydraulically operated, sidewall-mounted, injection system capable of injecting the model into the test section in less than 0.5 sec. The test article was mounted to a flat plate that, upon injection, became the test section sidewall. Before injection, the test article was stored in a housing which was isolated from the test section by a sliding door. A detailed description of this tunnel has previously been reported.[6]

Test Articles

The primary goal of this study was to determine the pressure-sensing performance of boundary-layer rakes without protruding pitot tubes. Test articles with cylindrical leading edges were chosen based on their generic shape, predictable pressure variation with flow angularity, and manufacturability. Figure 1 shows the four test articles. These articles were built 11 in. long to ensure that the top port holes were in the inviscid test section core.

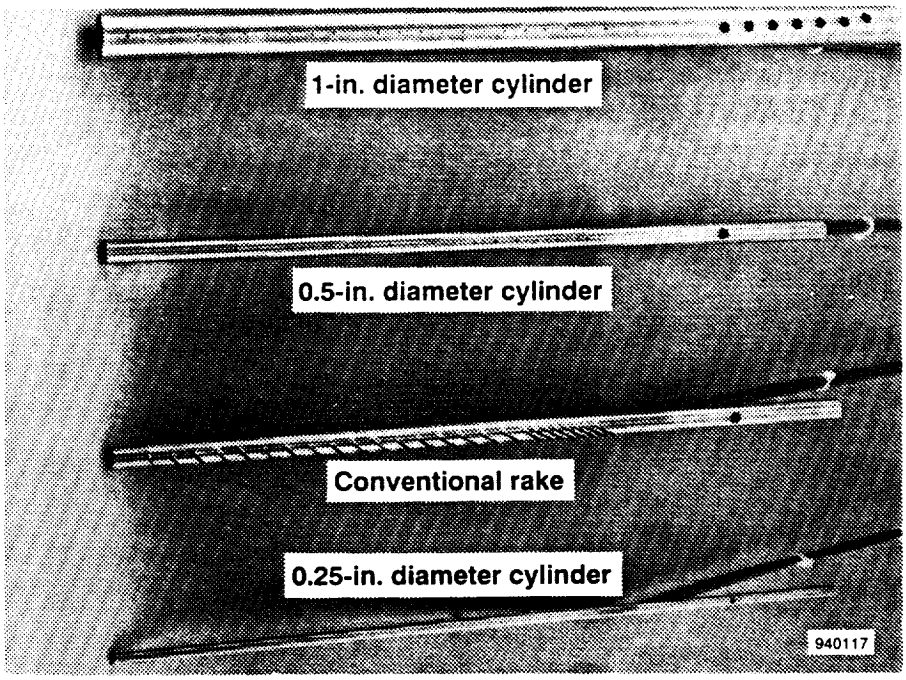

Figure 1. The four test articles.

Conventional Rake

For this study, the conventional rake is defined as the boundary-layer rake with protruding pitot tubes. The conventional rake had twenty-five 0.06 in. outer diameter (OD) and 0.04 in. inner diameter (ID) stainless steel protruding pitot tubes which extended 1.25 in. out from the 0.5-in. diameter cylinder. A pitot tube length of 1.25 in. was chosen to ensure that the pressure was measured upstream of any rake and wall interference effects.[7] The pitot tubes were spaced 0.25 in. apart along the length of the cylinder from its base to 2 in. above the wall. After 2 in., the pitot tubes were evenly spaced 0.5 in. apart along the remaining length of the cylinder. This spacing scheme was used to emphasize the region near the wall where any wall and cylinder interaction effects would be evident with the cylindrical test articles.

0.25-in. Diameter Cylinder

The 0.25-in. diameter cylinder rake had 21 flush-mounted, 0.02-in. diameter port holes evenly spaced 0.5 in. apart along the length of the cylinder. The smaller port holes and fewer port holes near the wall were employed as a result of structural and tubing mechanical restrictions.

0.5-in. Diameter Cylinder

The 0.5-in. diameter cylinder rake had an orifice layout that duplicated the conventional rake locations and ID size.

1-in. Diameter Cylinder

The 1-in. diameter cylinder rake had an orifice layout that duplicated the 0.25-in. diameter cylinder. All but one of the orifice holes were 0.04 ID. One orifice hole, at a location 9.5 in. above the wall, was

fitted with a 0.02 ID. In addition, seven orifice holes were installed at approximately –80°, –40°, –20°, 0°, 20°, 40°, and 80° around the circumference (reference to centerline) 4 in. above the wall for flow angularity information (fig. 2). After installation, the hole positions were measured and found to be at –79.50°, –40°, –19°, 0°, 20.25°, 41.50°, and 80° with an accuracy of ±0.15°.

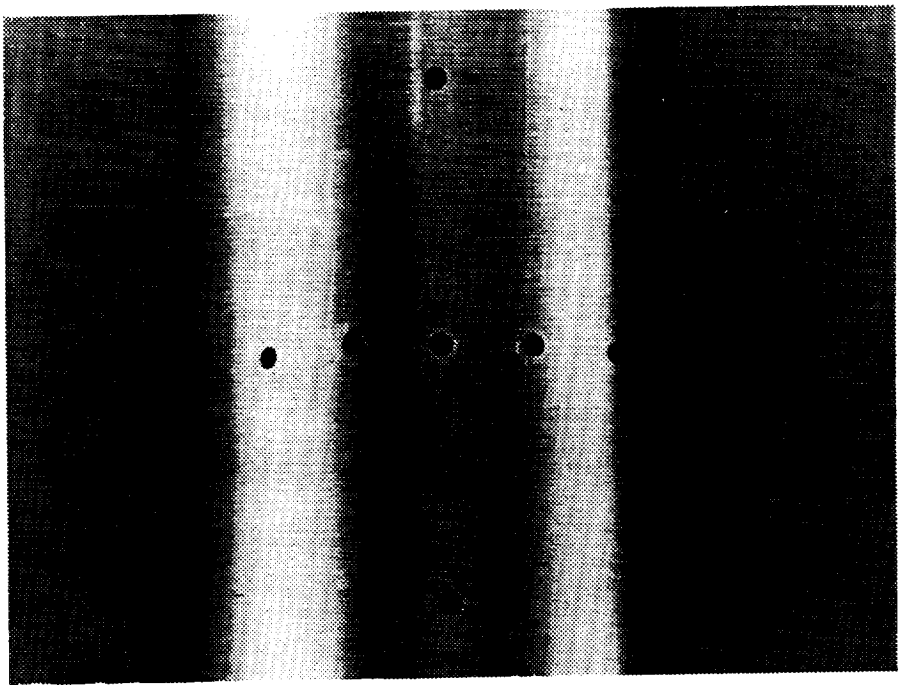

93-08145
(NASA Langley)

Figure 2. Circumferential pressure ports on the 1-in. diameter cylinder

Wall Static Pressures

To examine wall and cylinder interaction effects, a series of static pressure orifices were installed on the test section sidewall upstream of the test article attachment location. Eight static pressure orifices were located 0.62, 1.24, 1.85, 3.35, 4.85, 6.35, 7.85, and 9.35 in. in-line and upstream of the test articles.

Instrumentation

Rake and test section sidewall pressures were measured by electronically scanned pressure (ESP) silicon sensors. These ESP modules contained 32 sensors and were located on the backside of the sidewall injection system to minimize tubing length and, hence, settling (lag) time. A pneumatically controlled slide allowed the transducers to be calibrated on-line. This on-line calibration consisted of applying five known pressures which spanned the range of expected measured pressures. In anticipation of the widely differing pressure ranges on the test articles and tunnel sidewall and to ensure the best resolution, the pressure orifices were connected to modules rated for either 0.36 or 5 psi. An absolute pressure gauge rated at 2000 psi was used to measure the settling chamber reservoir pressure.

Pressure Measurement Uncertainty

Manufacturer specifications indicate that the precision of the 0.36- and 5-psi ESP gauges was ±0.1 and ±0.05 percent full scale, respectively. The precision of the 2000 psi gauge was ±0.01 percent full scale. All the pressures presented were normalized by the settling chamber reservoir pressure to remove any run-to-run and time-varying facility pressure variations. A standard uncertainty analysis was performed on the pressure ratios using the aforementioned precision values. The largest amount of measurement uncertainty occurred at the lowest Reynolds number of 0.5 million/ft where the lowest pressures are generated. Under this condition, the relative uncertainty for the test article pressure ratio was 0.2 percent for orifices using the 5-psi ESP gauge and 1.5 percent for orifices using the 0.36-psi ESP gauge. Uncertainty in the wall pressure ratio was 3.1 percent.

Test Procedures

The test articles were mounted upright on the sidewall of the test section of the NASA Langley 31 Inch Mach 10 Wind Tunnel. The conventional rake was tested first. For a typical run, the reservoir air was heated, and the reservoir pressure was set to produce the required test section unit Reynolds number. A control valve was opened, and the tunnel was started. Then, the test article was injected into the test section, and the test section pressure was allowed to stabilize before data were acquired. Total run times were on the order of 20 sec. Results were obtained by averaging the data over the last 3 sec of the stabilized run time.

RESULTS AND DISCUSSION

The overall goal of this study was to determine the pressure-sensing performance of upright cylinders in a Mach 10 boundary layer. To accomplish this goal, the experiment investigated four major areas which could affect the boundary-layer pressures of an upright cylinder: cylinder diameter, Reynolds number, flow angularity, and shock wave impingement. Because of the fixed geometry of the nozzle throat and test section, only a free-stream Mach number of 10 was investigated. Table 1 lists the tunnel operating conditions for these tests. The boundary-layer pressure ratios, wall pressure ratios, and flow angularity results are tabulated in tables 2, 3, and 4. The effects of the four areas under investigation are described in the next subsections.

Effect of Cylinder Diameter on Boundary-Layer Pressures

The conventional rake pitot pressure survey was compared to the boundary-layer pressures measured on the 0.25-, 0.5-, and 1-in. diameter cylinders at a free-stream Reynolds number of 2 million/ft. Figure 3 shows an overall view of the boundary layer. All pressures were normalized by the wind tunnel reservoir pressure that was measured in the settling chamber, located upstream of the nozzle throat. Boundary-layer pressures of the three cylindrical test articles showed little deviation from the conventional rake pitot pressures across the approximately 8-in. boundary-layer thickness (fig. 3). For this study, boundary-layer thickness was defined as the location where the pressure ratio was 95 percent of the predicted test section pressure ratio. Because of the slight nonuniformity of the pressures across the test section, boundary-layer edge pressures did not converge to a single value (as they would in a flight environment). Because the pressures across the complete test section were not measured, the approximate test section pressure ratios at the various wind tunnel operating conditions were obtained from a previous wind tunnel calibration study.[8]

Table 1. Pressure profile and flow angularity test conditions.

(a) Pressure profile comparison.

Case	Test article	Reynolds number, million/ft	Mach $_\infty$	P_o, psi	T_o, °R
1	Conventional rake	0.5	10	351.6	1791.2
2	Cylinder, 0.5 in.	0.5	10	350.4	1783.2
3	Conventional rake	1	10	717.0	1816.8
4	Cylinder, 0.5 in.	1	10	733.8	1785.8
5	Cylinder, 1 in.	1	10	731.8	1809.7
6	Cylinder with wedge, 1 in.	1	10	723.5	1780.5
7	Conventional rake	2	10	1455.2	1822.3
8	Cylinder, 0.25 in.	2	10	1454.7	1823.2
9	Cylinder, 0.5 in.	2	10	1446.7	1814.4
10	Cylinder, 1 in.	2	10	1453.0	1802.7

(b) Flow angularity for a 1-in. cylinder.

Case	Pivot, deg	Reynolds number, million/ft	Mach $_\infty$	P_o, psi	T_o, °R
11	0	1	10	731.8	1809.7
12	2	1	10	721.1	1795.8
13	4	1	10	721.3	1798.4
14	6	1	10	724.4	1768.6
15	8	1	10	721.2	1785.7
16	10	1	10	721.1	1823.8

Table 2. Measured boundary-layer pressures normalized by the wind tunnel reservoir pressure.

	Case									
Distance, in.	1	2	3	4	5	6	7	8	9	10
10.50	0.0032528	0.0032534	0.0031132	0.0030984	0.0031154	0.0031112	0.0029587	0.0029553	0.0029607	0.0029580
10.00	0.0031919	0.0032079	0.0030615	0.0030535	0.0030721	0.0030607	0.0028969	0.0028998	0.0029090	0.0029061
9.50	0.0031140	0.0031380	0.0030033	0.0029916	0.0030008	0.0029992	0.0028651	0.0028684	0.0028731	0.0028671
9.00	0.0029989	0.0030289	0.0029303	0.0029152	0.0029222	0.0029247	0.0028465	0.0028389	0.0028365	0.0028337
8.50	0.0027699	0.0027896	0.0028420	0.0027978	0.0028458	0.0028389	0.0028058	0.0027880	0.0027663	0.0027719
8.00	0.0024806	0.0025204	0.0026591	0.0026166	0.0026926	0.0026610	0.0027346	0.0026978	0.0026530	0.0026600
7.50	0.0022203	0.0022691	0.0024252	0.0023933	0.0024878	0.0024535	0.0025236	0.0025446	0.0025031	0.0024779
7.00	0.0018950	0.0019150	0.0021548	0.0021547	0.0022385	0.0022099	0.0022456	0.0022941	0.0022623	0.0022274
6.50	0.0015223	0.0015451	0.0017604	0.0017640	0.0018143	0.0017577	0.0019758	0.0020010	0.0019727	0.0019288
6.00	0.0011926	0.0012135	0.0013805	0.0014038	0.0014527	0.0020051	0.0015223	0.0015721	0.0015330	0.0015577
5.50	0.00094824	0.00097408	0.0010861	0.0011172	0.0011467	0.0012713	0.0012179	0.0012433	0.0012319	0.0012502
5.00	0.00077747	0.00078690	0.00086934	0.00088682	0.00089688	0.00074734	0.00098068	0.00099365	0.00098850	0.0010068
4.50	0.00061614	0.00062563	0.00068960	0.00070072	0.00072062	0.00049255	0.00075646	0.00077673	0.00076922	0.00079045
4.00	0.00050023	0.00051084	0.00056074	0.00056260	0.00058849	0.00035108	0.00061402	0.00061486	0.00060968	0.00063102
3.50	0.00041929	0.00042315	0.00045951	0.00046336	0.00046293	0.00025596	0.00051664	0.00051350	0.00050571	0.00051674
3.00	0.00035860	0.00035729	0.00037987	0.00038366	0.00037816	0.00025550	0.00043934	0.00043447	0.00043158	0.00043130
2.50	0.00028107	0.00030138	0.00031210	0.00031814	0.00032689	0.00022436	0.00035162	0.00036118	0.00035920	0.00036145
2.00	0.00023800	0.00025627	0.00026541	0.00026994	0.00032225	0.00010599	0.00029086	0.00029983	0.00029621	0.00031975
1.75	0.00021629	0.00023806	0.00024340	0.00025004	---	---	0.00026425	---	0.00027101	---
1.50	0.00023072	0.00024366	0.00023247	0.00025196	0.00027873	7.6564e-05	0.00024494	0.00025432	0.00025465	0.00027870
1.25	0.00021016	0.00021989	0.00021447	0.00023726	---	---	0.00022266	---	0.00024188	---
1.00	0.00018841	0.00019217	0.00019729	0.00021688	0.00019393	7.8671e-05	0.00020216	0.00020767	0.00022922	0.00020551
0.75	0.00016461	0.0015569	0.00017952	0.00018733	---	---	0.00018470	---	0.00020170	---
0.50	0.00012313	0.00010713	0.00015257	0.00014287	0.00011561	7.6884e-05	0.00016328	0.00016814	0.00015272	0.00010959
0.25	7.0078e-05	6.7452e-05	9.4484e-05	7.8846e-05	---	---	0.00012048	---	8.9081e-05	---

Table 3. Measured wall pressures normalized by the wind tunnel reservoir pressure.

	Case			
Distance, in.	4	8	9	10
–0.620	3.2216e-05	3.0149e-05	3.5389e-05	4.1990e-05
–1.24	3.2591e-05	2.6433e-05	3.2477e-05	3.9000e-05
–1.85	3.1951e-05	2.3811e-05	2.7589e-05	3.3997e-05
–3.35	3.3925e-05	2.3794e-05	2.5062e-05	2.8510e-05
–4.85	3.1751e-05	2.4142e-05	2.5939e-05	2.5421e-05
–6.35	3.3319e-05	2.3842e-05	2.5208e-05	2.4725e-05
–7.85	3.7078e-05	2.3876e-05	2.5242e-05	2.4655e-05
–9.35	4.1465e-05	2.4007e-05	2.5736e-05	2.5044e-05

Table 4. Measured pressures at various flow angles normalized by the wind tunnel reservoir pressure for a 1-in. cylinder, 4 in. above the wall.

Flow angle, deg	Pressure ratio	Case
90.00	6.7649e-05	16
88.00	7.1280e-05	15
86.00	8.4922e-05	14
84.00	8.4105e-05	13
82.00	9.3523e-05	12
80.00	0.00010933	11
79.50	0.00011565	11
77.50	0.00011330	12
75.50	0.00012092	13
73.50	0.00013648	14
71.50	0.00014187	15
69.50	0.00015334	16
51.50	0.00025855	16
49.50	0.00027122	15
47.50	0.00028371	14
45.50	0.00030534	13

Table 4. Concluded.

Flow angle, deg	Pressure ratio	Case
43.50	0.00032466	12
41.50	0.00033804	11
40.00	0.00035833	11
38.00	0.00037334	12
36.00	0.00038909	13
34.00	0.00040256	14
32.00	0.00041772	15
30.00	0.00043467	16
28.25	0.00045572	15
26.25	0.00048402	14
24.25	0.00049201	13
22.25	000050926	12
20.25	0.00053254	11
19.00	0.00054221	11
17.00	0.00053063	12
15.00	0.00053449	13
13.00	0.00055305	14
11.00	0.00054043	15
10.00	0.00055791	16
9.00	0.00056009	16
8.00	0.00055300	15
6.00	0.00056570	14
4.00	0.00056629	13
2.00	0.00057237	12
0.00	0.00058849	11

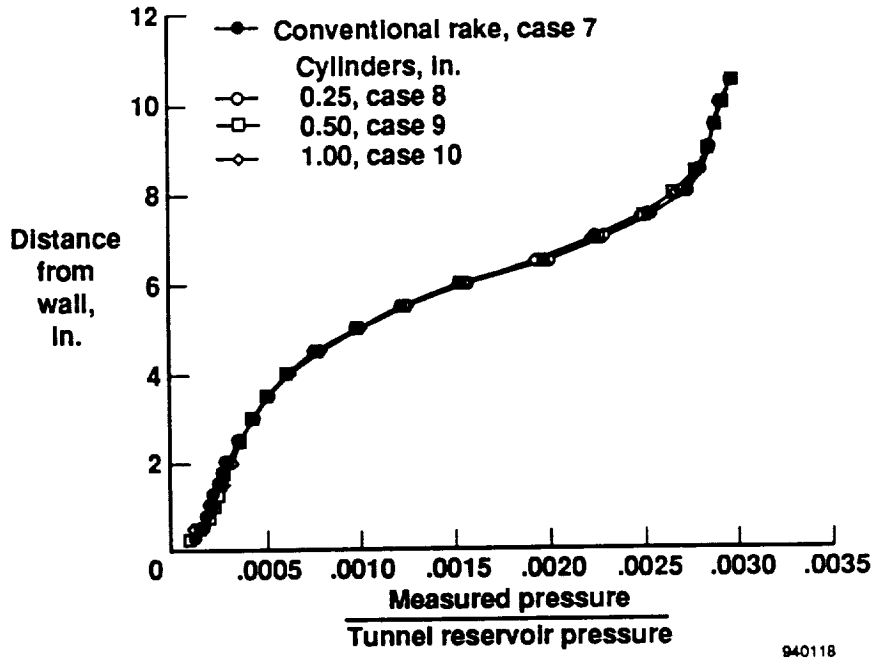

Figure 3. Comparison of conventional rake pressures to cylinder pressures. Reynolds number equals 2 million/ft.

The shallow shape of the measured boundary-layer pressure profile was ascribed to the vertically varying shock strength of the bow shock in front of the cylinder and arose in the following manner: The Mach number profile within the boundary layer created a varying shock wave pattern in front of the cylinder. This pattern was strongest at the top of the cylinder within the inviscid flow and became very weak near the wall (fig. 4). In addition, flow separation upstream of the wall and cylinder junction created a lambda-shock structure near the wall that influenced the measured pressures. In conjunction with the typical boundary-layer stagnation profile which existed upstream of the shock wave structure, these affects resulted in a shallow boundary-layer pressure profile (fig. 3).

Taking a closer look at the data within 3 in. of the wall, figure 5 shows a comparison of the conventional rake and cylinder pressures for the same conditions as those presented in figure 3. Here, the boundary-layer pressures of all three cylindrical test articles show significant deviation from the conventional rake pitot pressures. While the 0.25-in. diameter cylinder shows only little deviation near $y = 0.5$ in., the 0.5-in. diameter cylinder boundary-layer pressures were at most 29 percent less than the conventional rake pressures at $y < 0.5$ in. and were at most 12 percent higher than the conventional rake pressures from 0.5 in. $< y <$ 1.5 in. The same is true for the 1-in. diameter cylinder; only the deviations were larger and extended farther off the wall. The 1-in. cylinder boundary-layer pressures were at most 39 percent lower than the conventional rake pressures at $y < 1$ in. and were at most 13 percent higher than the conventional rake pressures from 1 in. $< y <$ 2.5 in. The pressure deviations seen on all cylindrical test articles resulted from a separation region that existed in front and "horseshoed" around the cylinders. The separation region contained a vortex (fig. 4) that circulated in such a way as to cause a suction close to the wall and cylinder interface and an increase in pressure in the upper half of the interaction.[9,10] As seen in figure 5, this interaction scales with diameter, with the largest diameter causing the largest interaction and the largest pressure deviations.

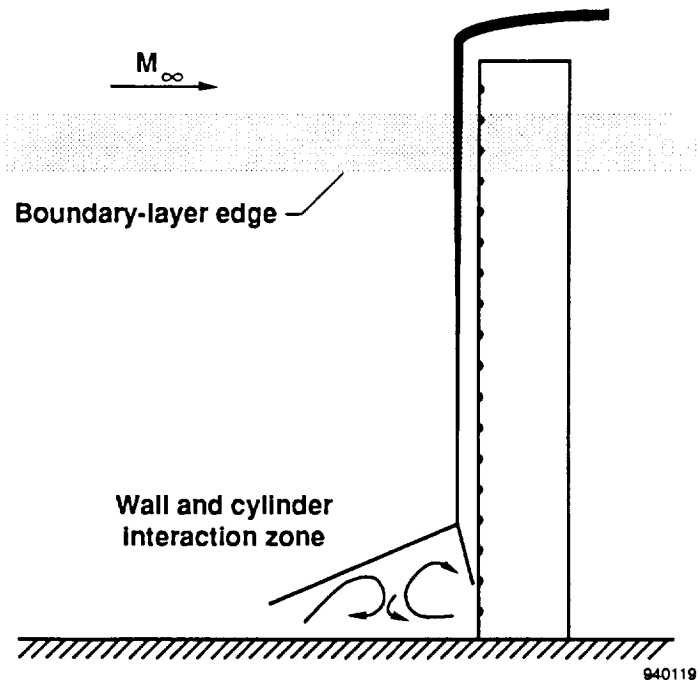

Figure 4. Shock wave pattern in front of the cylinder.[9]

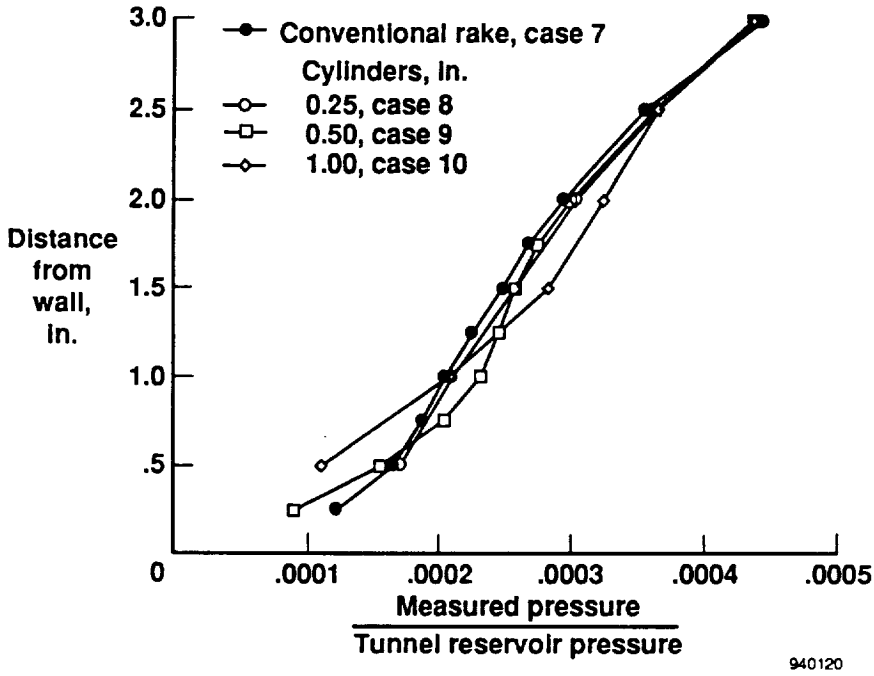

Figure 5. Comparison of conventional rake pressures and cylinder pressures. Reynolds number equals 2 million/ft.

Boundary-layer thickness-to-cylinder-diameter ratio undoubtedly plays a role in the pressure-sensing performance of an upright cylinder. This ratio dictates how large the upstream separation region and resulting horseshoe vortex will be in relation to the overall boundary-layer thickness. For the pressure profiles shown in figure 3, the 0.25-, 0.5-, and 1-in. diameter cylinders had a boundary-layer thickness-to-cylinder-diameter ratio of approximately 32, 16, and 8, respectively. The percent of boundary-layer thickness affected by the separation region for the various ratios was curve fit and found to increase as a power law for the conditions studied (eq. (1)). For this correlation, it was assumed that the separation region for the 0.25-in. diameter cylinder extended up to the lowest orifice, or 0.5 in. This assumption resulted in equation (1) being a conservative prediction. Reynolds number effects were negligible at the conditions studied.

$$y = 10^{(-0.03x+1.75)} \tag{1}$$

where

y = deviation thickness expressed as a percent of boundary-layer thickness

x = boundary-layer thickness-to-cylinder-diameter ratio

Note that equation (1) was not experimentally validated for boundary-layer thickness-to-cylinder-diameter ratios less than 8.

The affects of the separation region can also be seen on the wall static pressure distribution in front of the test articles. Figure 6 shows wall pressure normalized by tunnel reservoir pressure at locations upstream of the test article at a free-stream Reynolds number of 2 million/ft. For the three cylinders tested, the wall static pressure deviates from the typical wall value approximately 4 diameters upstream. Hence, the interaction footprint scales proportionally with cylinder diameter.

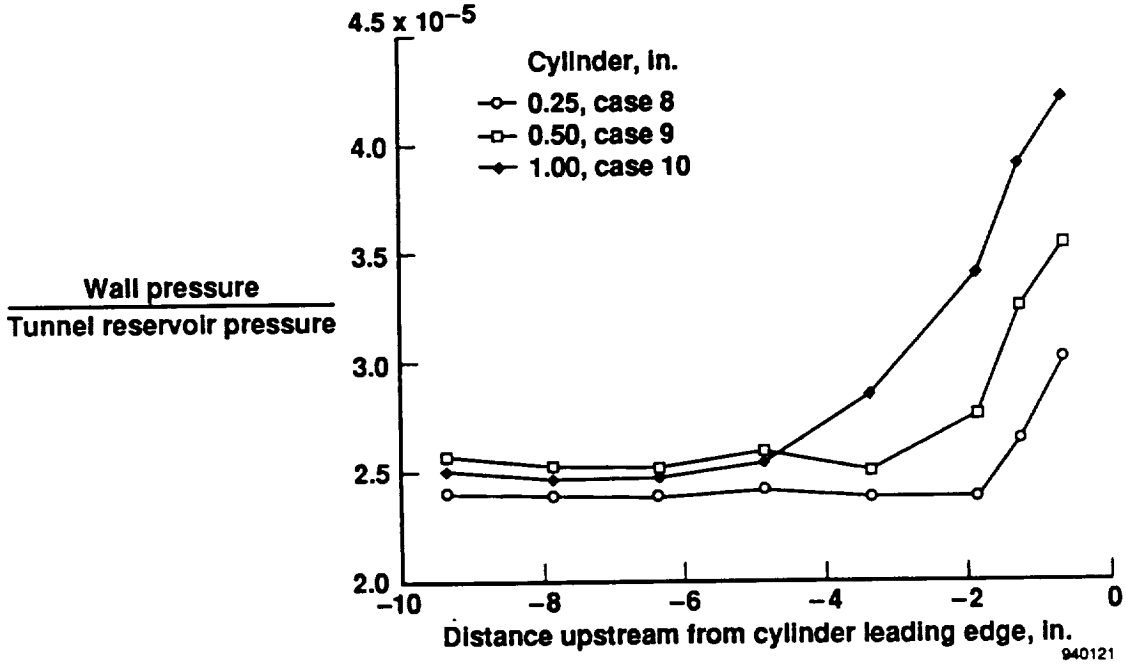

Figure 6. Effect of diameter on the wall static pressure upstream of the cylinders. Reynolds number equals 2 million/ft.

Effect of Reynolds Number on Boundary-Layer Pressures

Changes in Reynolds number in a turbulent boundary layer affect the boundary-layer thickness, separation, and reattachment. Determining if a change in Reynolds number has an affect on the boundary-layer pressure-sensing performance of an upright cylinder was of interest. The conventional rake pitot pressure survey was compared to the boundary-layer pressures measured on the 0.5-in. diameter cylinder at free-stream Reynolds numbers of 0.5, 1, and 2 million/ft in figures 7 and 8. Figure 7 shows an overall view of the boundary layer, and figure 8 examines the pressures near the wall. As seen in figure 7, the boundary-layer pressures of the three cylindrical test articles show little deviation from the conventional rake pitot pressures across the boundary-layer thickness. Here, it is evident that the boundary-layer thickness changes from approximately 9 in. at the free-stream Reynolds numbers of 0.5 million/ft (fig. 7(a)) to a thickness of approximately 8 in. at a free-stream Reynolds number of 2 million/ft (fig. 7(c)).

Taking a closer look at the data within 3 in. of the wall, figure 8 shows a comparison of the conventional rake pressures and the 0.5-in. cylinder pressures for the same data presented in figure 7. In figure 8(a), at a Reynolds number of 0.5 million/ft, an inflection point is evident in the pressure profiles of both test articles at $y = 1.5$ in. Such an inflection point is not apparent at the other Reynolds numbers. This inflection may result from facility-driven effects. The 0.5-million/ft Reynolds number is near the lowest operational unit Reynolds number for the NASA Langley 31 Inch Mach 10 Wind Tunnel. The shape of the boundary-layer pressure profile may be influenced by this off-design condition. Examining figure 8(b) at free-stream Reynolds number of 1 million/ft and figure 8(c) at a free-stream Reynolds number of 2 million/ft reveals little change in the deviation region.

This negligible effect of Reynolds number at 1 and 2 million/ft can also be seen on the wall static pressure distribution in front of the test articles. Figure 9 shows wall pressure normalized by tunnel reservoir pressure at locations upstream of the 0.5-in. diameter test article at free-stream Reynolds numbers of 1 and 2 million/ft. The wall static pressure deviates from the typical wall value approximately 2 in. upstream, or 4 diameters for each of these two cases. Reynolds number does not appear to affect the pressure-sensing performance of upright cylinders at Reynolds numbers of 1 and 2 million/ft significantly. Data at 0.5 million/ft are not presented because of the suspect pressure profile of the boundary layer.

Effect of Flow Angularity on Surface Pressure Distribution

Surface pressure distribution over a circular cylinder has been a thoroughly studied subject.[11] If the stagnation point of the flow is moved away from the position where the pressure orifices are located, a change in the measured boundary-layer pressure will result. If not understood and accounted for, this change in stagnation point will produce misleading boundary-layer pressure profiles. As a result, a seven-orifice pressure matrix was installed around the circumference of the leading edge of the 1-in. diameter cylinder to provide flow angularity information (fig. 2). The orifices were installed in-line at a location 4 in. above the tunnel wall and were well within the viscous flow region of the wind tunnel boundary layer.

Figure 10 shows the effect of flow angularity on the surface pressure distribution of the 1-in. diameter cylinder at a free-stream Reynolds number of 1 million/ft. Additional data points were acquired by pivoting the cylinder by 2°, 4°, 6°, 8°, and 10° and computing the total flow angle for each orifice. Once again, all pressures were normalized by the wind tunnel reservoir pressure. The typical cosine-shaped pressure distribution was measured on the cylinder where the 0° position was at the stagnation point. Flow angles of less than 10° changed the pressure ratio by less than approximately 5 percent. Angles greater than 10° resulted in much greater differences. For example at approximately 25°, the pressure ratio was approximately 18 percent different from that which occurred at the 0° position.

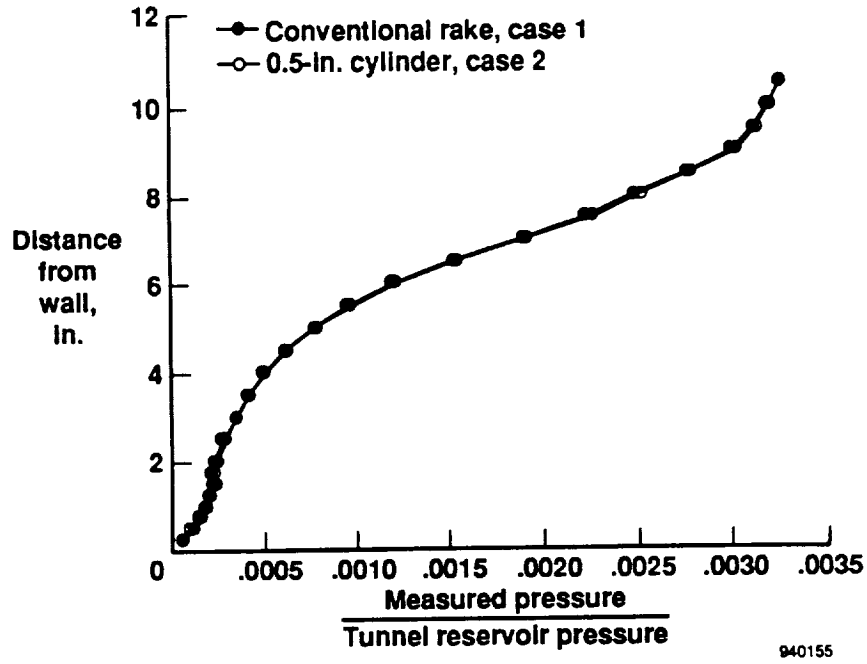

(a) Reynolds number equals 0.5 million/ft.

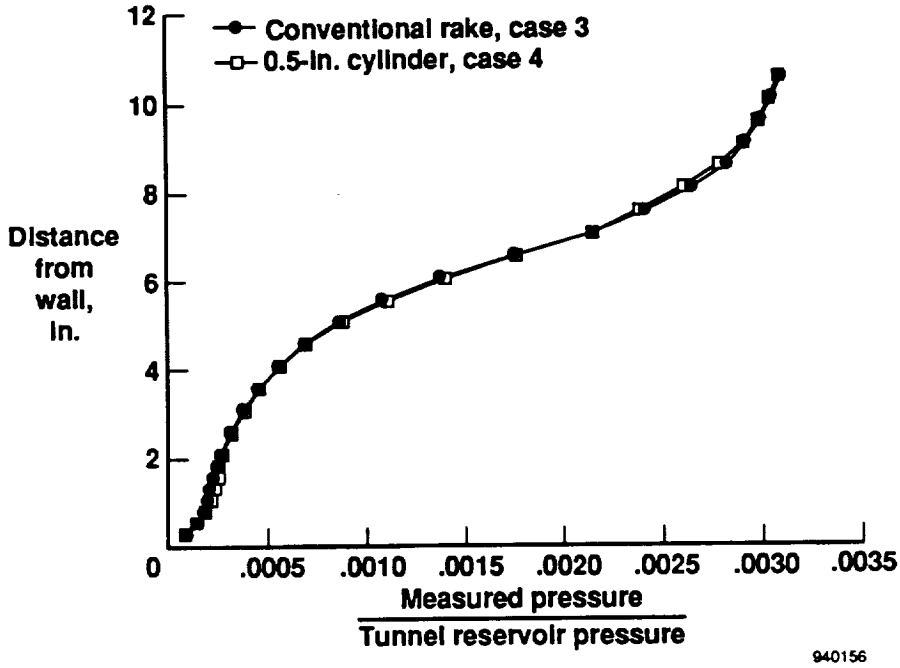

(b) Reynolds number equals 1 million/ft.

Figure 7. Effect of Reynolds number on boundary-layer surveys using a 0.5-in. diameter cylinder.

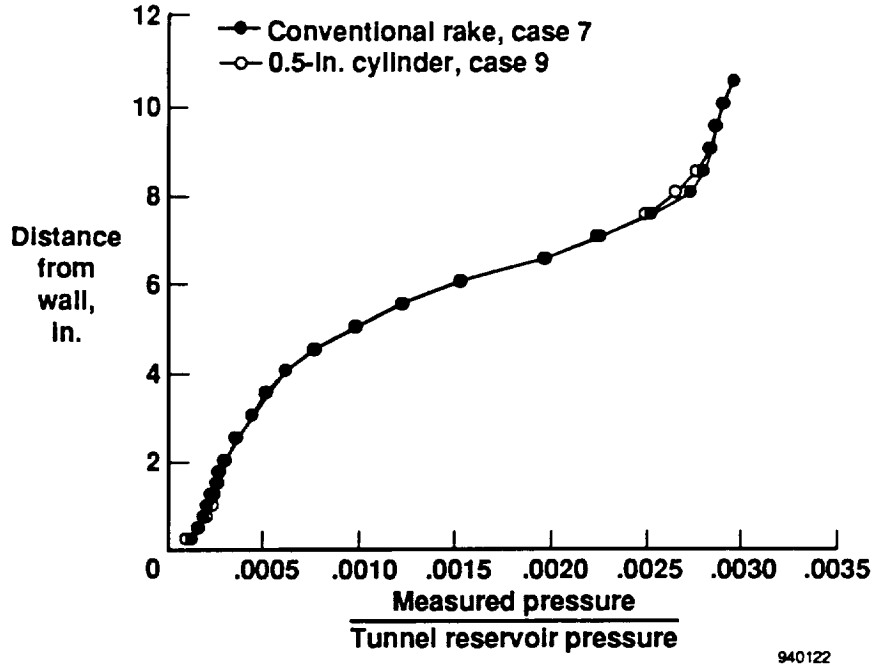

(c) Reynolds number equals 2 million/ft.

Figure 7. Concluded

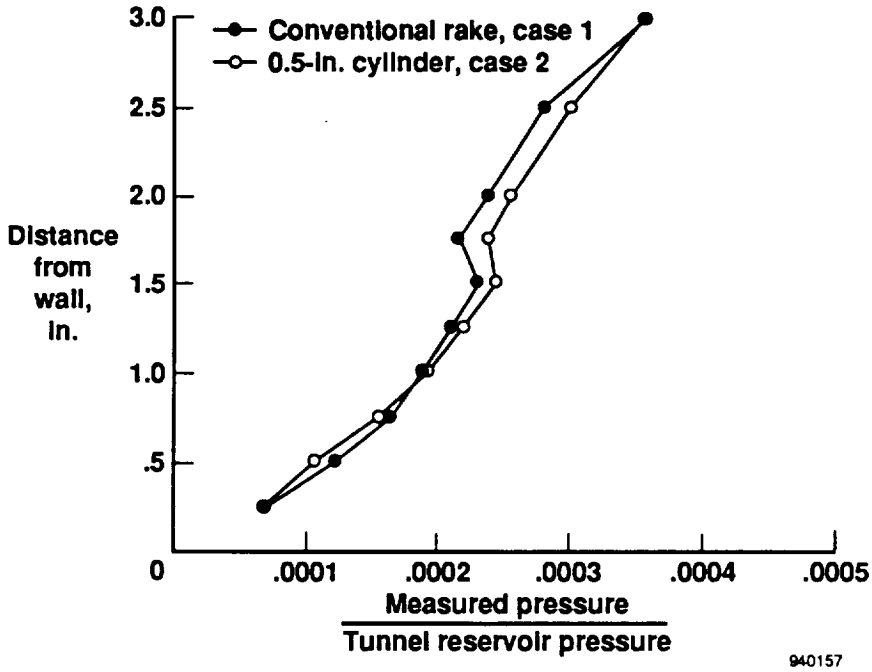

(a) Reynolds number equals 0.5 million/ft.

Figure 8. A closer look near the wall. Effect of Reynolds number on boundary-layer surveys using a 0.5-in. diameter cylinder.

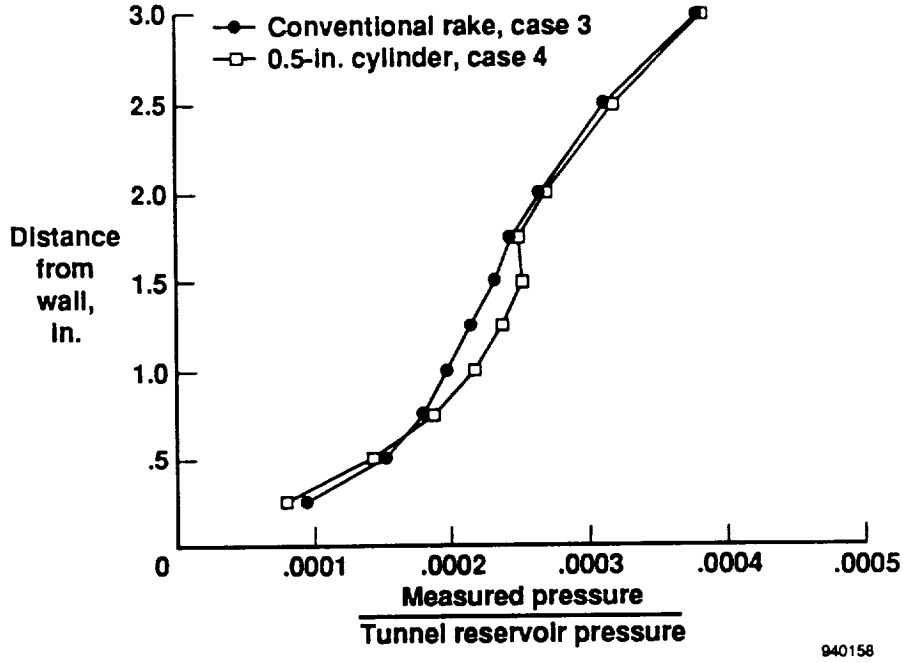

(b) Reynolds number equals 1 million/ft.

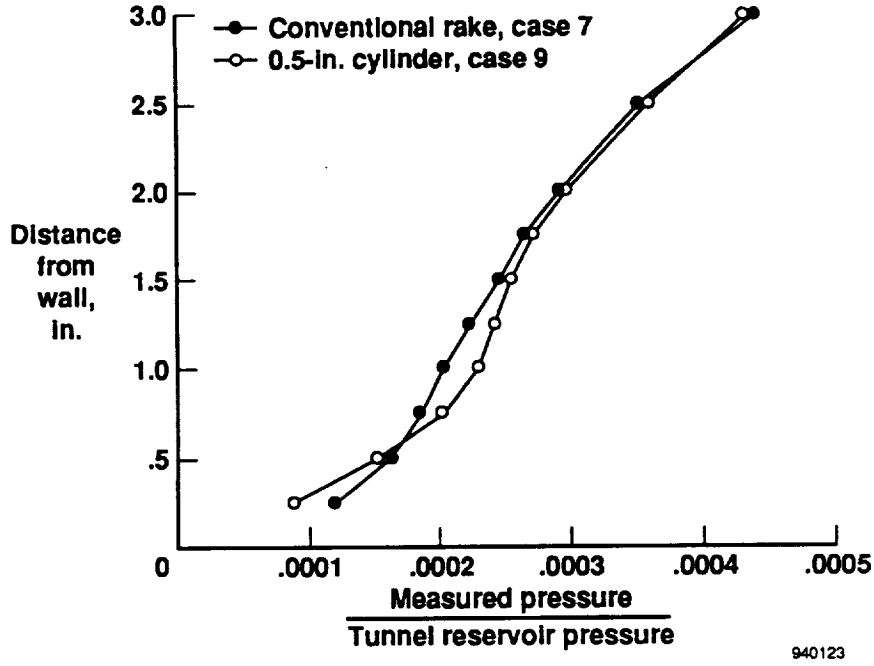

(c) Reynolds number equals 2 million/ft.

Figure 8. Concluded.

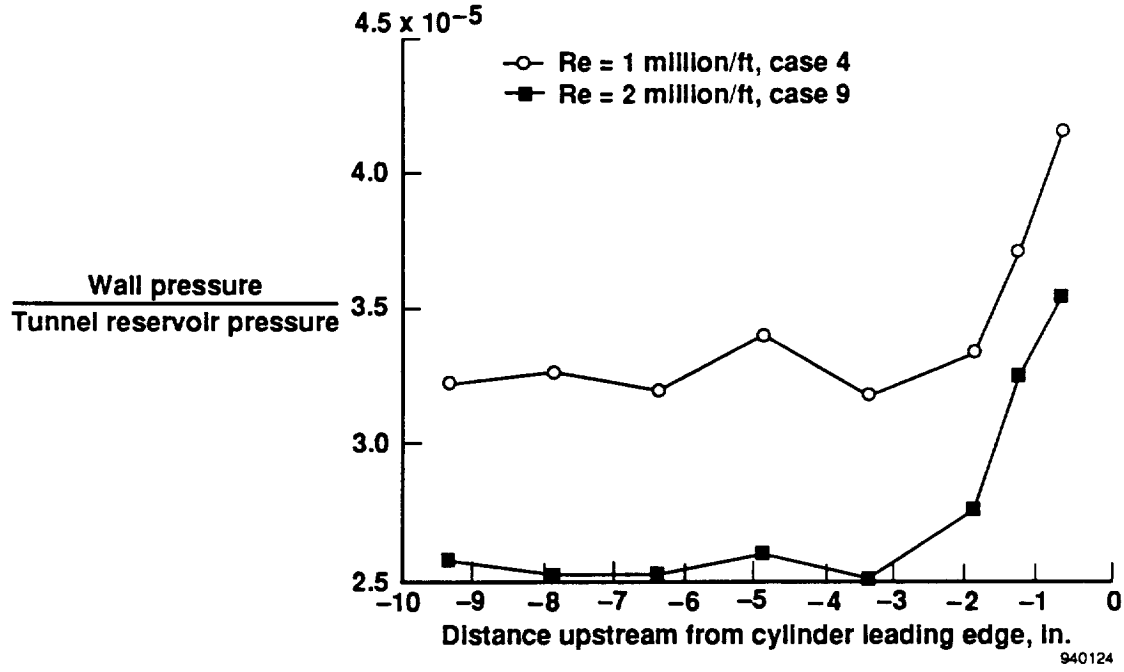

Figure 9. Effect of Reynolds number on the wall static pressure upstream of the 0.5-in. diameter cylinder.

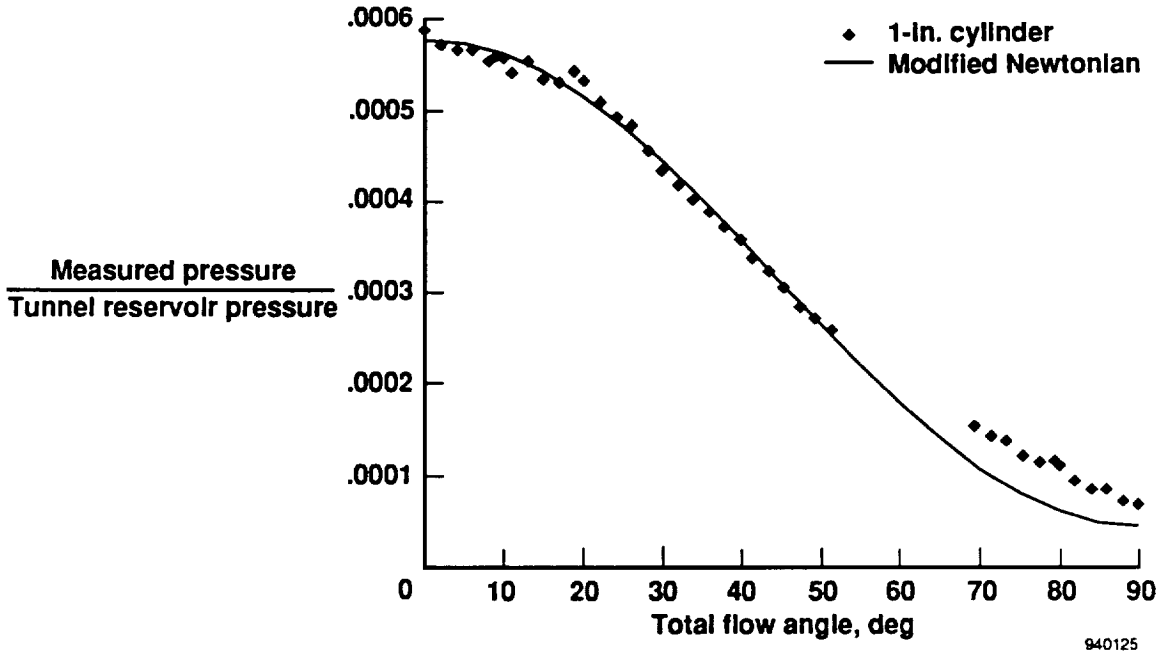

Figure 10. Surface pressure distribution for flow past the 1-in. diameter cylinder. At 4 in. above the wall, $\gamma = 1.4$, and boundary-layer Mach number = 3.1.

Figure 10 also shows the prediction for the pressure distribution over a circular cylinder based on modified Newtonian theory.[11] Even within the boundary layer where the incoming Mach number was calculated to be 3.1, the surface pressure distribution behaved very Newtonian up to a flow angle of 50°. After 50°, the measured pressures were significantly higher than the predictions.

Speculation exists that flow angularity can be determined using a seven-orifice pressure matrix and the modeling and analysis technique developed for subsonic aircraft applications.[12] In addition, based on modified Newtonian theory and the flow angularity information, the stagnation pressure can be determined. Thus, the measured pressure profile can be corrected for flow angularity effects, and a representative zero-flow angularity pressure profile can be determined. The accuracy of such a technique is an area for further study.

Effect of Shock Wave Impingement on Boundary-Layer Pressures

A boundary-layer probe without protruding tubing may be susceptible to orifice crosstalk. Although the presented boundary-layer pressure profile comparisons have shown no evidence of orifice crosstalk, a more conclusive test would be to impinge an oblique shock wave on the cylinder, thereby generating a discrete pressure jump at one location on the probe. To generate an oblique shock and test for crosstalk, a 30° wedge that was 3 in. wide and 2 in. tall was placed 12 in. in-line and upstream of the 1-in. diameter cylinder. The wave produced from the 30° wedge was estimated to intersect the cylinder 6 in. above the wall. Figure 11 shows the 30° wedge, shock wave, and shock wave impingement on the 1-in. diameter cylinder.

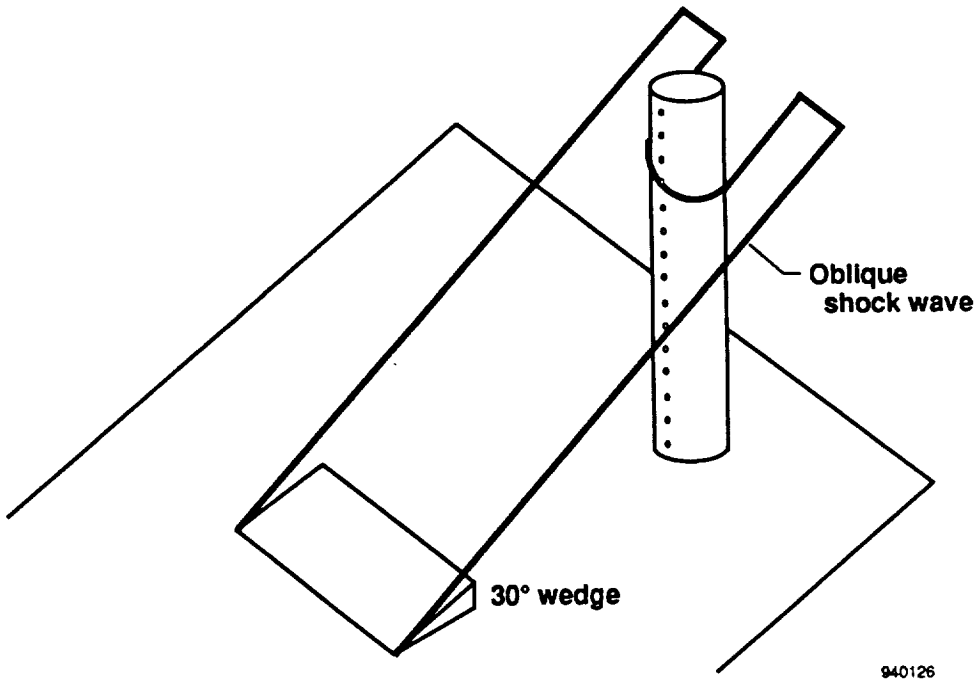

Figure 11. Shock wave impingement.

Figure 12 shows the effect of shock wave impingement on the leading-edge pressures of the 1-in. diameter cylinder at a free-stream Reynolds number of 1 million/ft. Here, the 1-in. diameter cylinder boundary-layer pressures (with no upstream wedge) are compared to the boundary-layer pressures with

the 30° wedge installed in-line and upstream. At a location 6 in. above the wind tunnel test section side wall, the shock wave causes a sharp increase in pressure. This increase results from the flow being more efficiently compressed (increased pressure recovery) by an oblique shock and then a normal shock as compared to just a normal bow shock in the baseline case. Note that the pressure measured above the oblique shock impingement showed no influence of the increase in pressure seen by the lower port location. Hence, no orifice crosstalk was evident at the conditions studied. The distorted pressure profile below 5 in. was caused by the wake of the shock-generating wedge.

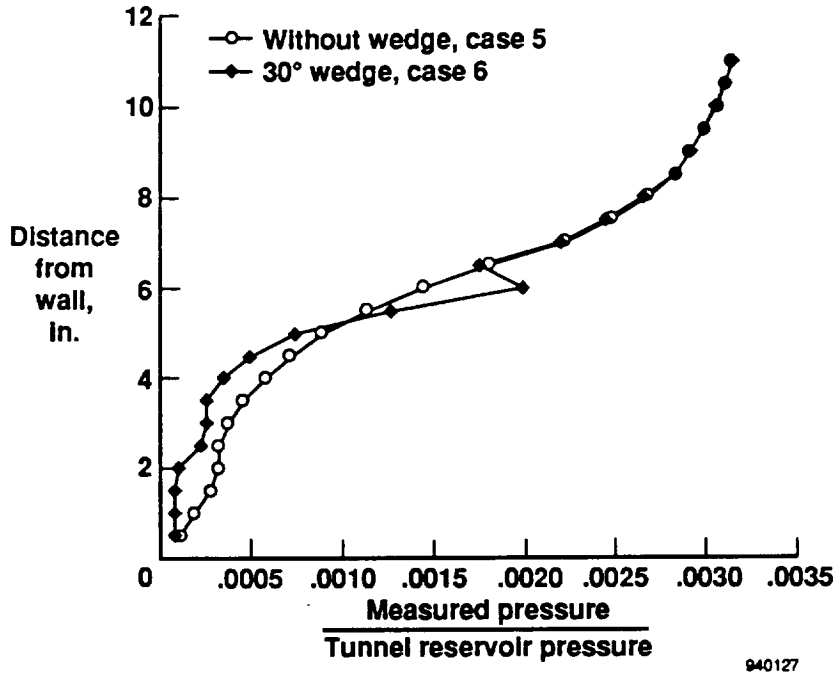

Figure 12. Effect of shock wave impingement on pressure measurement. Reynolds number equals 1 million/ft.

CONCLUSIONS

This study investigated the pressure-sensing performance of upright cylinders in a Mach 10 hypersonic boundary layer. Boundary-layer pressure profiles measured on the leading edges of 0.25-, 0.5-, and 1-in. diameter cylinders were compared to conventional rake measurements over a free-stream Reynolds number range of 0.5 to 2 million/ft. The ultimate aim was to provide quantitative accuracy information to be used in determining the feasibility of using a rake without protruding pitot tubes to measure hypersonic boundary-layer pressure profiles. The effect of flow angularity and shock wave impingement on the cylinder leading-edge pressure measurement was also investigated. Some of the more salient conclusions derived from these measurements are listed next.

1. An upright ported cylinder can be used to measure boundary-layer pressure profiles in a hypersonic boundary layer.

2. The ratio of boundary-layer thickness to cylinder diameter plays an important role in the pressure-sensing performance. A separation region is generated near the wall and cylinder junction and

scales with the ratio of boundary-layer thickness to cylinder diameter. A boundary-layer thickness-to-cylinder-diameter ratio of 8 proved sufficient to determine an overall pressure profile and ascertain the boundary-layer thickness. An empirical equation was determined that computes the percent of boundary-layer thickness affected by the separation region.

3. The Reynolds number does not appear to affect the pressure-sensing performance of upright cylinders over a range of Reynolds numbers from 1 to 2 million/ft significantly.

4. The affect of flow angularity on pressure measurement is very dramatic. The typical cosine-shaped pressure distribution was measured on the cylinder. Thus in environments where flow angularity exists, the flow angularity must be determined. In addition, the measured pressure profile must be corrected to obtain the zero-flow angle pressure profile.

5. An oblique shock wave was impinged on the leading edge of the 1-in. diameter cylinder to investigate orifice crosstalk. That is the situation where a low pressure measured at one flush orifice on a boundary-layer probe may be influenced by a high pressure measured at another flush orifice. The lower pressure measured above the oblique shock impingement showed no influence of the increase in pressure generated at the lower port location. Hence, no orifice crosstalk was evident at the conditions studied.

Based on these study results, some recommendations on the use of an upright cylinder to measure hypersonic boundary-layer pressure profiles may be made. A boundary-layer thickness-to-cylinder-diameter ratio of 8 proved sufficient to measure an overall pressure profile and ascertain the boundary-layer thickness. Unfortunately, the separation region generated near the wall and cylinder junction introduced pressure inaccuracies that made the profile shape near the wall unlike the true profile. Any information gleaned from this region would have a large amount of uncertainty. Finally, in an environment of unknown flow angularity, a circumferential pressure orifice matrix is required. In this manner, the measured profile can be corrected for flow angularity effects. Accuracy of such a technique is an area for further study.

Dryden Flight Research Center
National Aeronautics and Space Administration
Edwards, California, March 1, 1994

REFERENCES

[1]Fisher, David F. and Edwin J. Saltzman, *Local Skin Friction Coefficients and Boundary-Layer Profiles Obtained in flight from the XB-70-1 Airplane at Mach Numbers up to 2.5*, NASA TN D-7220, 1973.

[2]Powers, Sheryll Goecke, *Flight-Measured Pressure Characteristics of Aft-Facing Steps in High Reynolds Number Flow at Mach Numbers of 2.20, 2.50, and 2.80 and Comparison with Other Data*, NASA TM-72855, 1978.

[3]Quinn, Robert D. and Leslie Gong, *In-Flight Boundary-Layer Measurements on a Hollow Cylinder at a Mach Number of 3.0*, NASA TP-1764, 1980.

[4]Quinn, Robert D. and Murray Palitz, *Comparison of Measured and Calculated Turbulent Heat Transfer on the X-15 Airplane at Angles of Attack up to 19.0°*, NASA TM X-1291, 1966.

[5]Keener, Earl R. and Edward J. Hopkins, *Accuracy of Pitot-Pressure Rakes for Turbulent Boundary-Layer Measurements in Supersonic Flow*, NASA TN D-6229, 1971.

[6]Miller, C.G., III, "Langley Hypersonic Aerodynamic/Aerothermodynamic Testing Capabilities—Present and Future," AIAA 90-1376, June 1990.

[7]Westkaemper, J.C., "Turbulent Boundary-Layer Separation Ahead of Cylinders," *AIAA Journal*, vol. 6, no. 7, July 1968, pp. 1352–1355.

[8]Miller, Charles G. III, *Measured Pressure Distributions, Aerodynamic Coefficients, and Shock Shapes on Blunt Bodies at Incidence in Hypersonic Air and CF_4*, NASA TM-84489, 1982.

[9]Kaufman, Louis G., II, Robert H. Korkegi, and Leo C. Morton, *Shock Impingement Caused by Boundary-Layer Separation Ahead of Blunt Fins*, ARL 72-0118, Aug. 1972.

[10]Couch, Lana M., *Flow-Field Measurements Downstream of Two Protuberances in a Flat Plate Submerged in a Turbulent Boundary Layer at Mach 2.49 and 4.44*, NASA TN D-5297, 1969.

[11]Anderson, John D., Jr., *Hypersonic and High Temperature Gas Dynamics*, New York, McGraw-Hill, 1989.

[12]Whitmore, S.A., T.R. Moes, M.W. Czerniejewski, and D.A. Nichols, *Application of a Flush Air-data Sensing System to a Wing Leading Edge (LE-FADS)*, NASA TM-104267, 1993.

REPORT DOCUMENTATION PAGE

Form Approved
OMB No. 0704-0188

1. AGENCY USE ONLY (Leave blank)	2. REPORT DATE	3. REPORT TYPE AND DATES COVERED
	July 1994	Technical Memorandum

4. TITLE AND SUBTITLE

Pressure-Sensing Performance of Upright Cylinders in a Mach 10 Boundary-Layer

5. FUNDING NUMBERS

WU 505-70

6. AUTHOR(S)

Steven Johnson and Kelly Murphy

7. PERFORMING ORGANIZATION NAME(S) AND ADDRESS(ES)

NASA Dryden Flight Research Center
P.O. Box 273
Edwards, California 93523-0273

8. PERFORMING ORGANIZATION REPORT NUMBER

H-1977

9. SPONSORING/MONOTORING AGENCY NAME(S) AND ADDRESS(ES)

National Aeronautics and Space Administration
Washington, DC 20546-0001

10. SPONSORING/MONITORING AGENCY REPORT NUMBER

NASA TM-4633

11. SUPPLEMENTARY NOTES

Kelly Murphy is affiliated with NASA Langley Research Center, Hampton, Virginia 23665-5225

12a. DISTRIBUTION/AVAILABILITY STATEMENT

Unclassified—Unlimited
Subject Category 02

12b. DISTRIBUTION CODE

13. ABSTRACT (Maximum 200 words)

An experimental research program to provide basic knowledge of the pressure-sensing performance of upright, flush-ported cylinders in a hypersonic boundary layer is described. Three upright cylinders of 0.25-, 0.5-, and 1-in. diameters and a conventional rake were placed in the test section sidewall boundary layer of the 31 Inch Mach 10 Wind Tunnel at NASA Langley Research Center, Hampton, Virginia. Boundary-layer pressures from these cylinders were compared to those measured with a conventional rake. A boundary-layer thickness-to-cylinder-diameter ratio of 8 proved sufficient to accurately measure an overall pressure profile and ascertain the boundary-layer thickness. Effects of Reynolds number, flow angularity, and shock wave impingement on pressure measurement were also investigated. Although Reynolds number effects were negligible at the conditions studied, flow angularity above 10° significantly affects the measured pressures. Shock wave impingement was used to investigate orifice-to-orifice pressure crosstalk. No crosstalk was measured. The lower pressure measured above the oblique shock wave impingement showed no influence of the higher pressure generated at the lower port locations.

14. SUBJECT TERMS

Boundary-layer measurements, Flow angularity, Hypersonic aerodynamics, Shock wave impingements, Upright cylinders, Wind tunnel tests

15. NUMBER OF PAGES

26

16. PRICE CODE

A03

17. SECURITY CLASSIFICATION OF REPORT	18. SECURITY CLASSIFICATION OF THIS PAGE	19. SECURITY CLASSIFICATION OF ABSTRACT	20. LIMITATION OF ABSTRACT
Unclassified	Unclassified	Unclassified	Unlimited

NSN 7540-01-280-5500

Available from the NASA Center for AeroSpace Information, 800 Elkridge Landing Road, Linthicum Heights, MD 21090; (301)621-0390

Standard Form 298 (Rev. 2-89)
Prescribed by ANSI Std. Z39-18
298-102